Proton spectroscopic factor of the ^{12}C ground state from the ^{12}C(^{11}B, ^{12}C)^{11}B elastic transfer reaction

E. T. Li (李二涛),[1] Z. H. Li (李志宏),[2,*] Y. J. Li (李云居),[2] B. Guo (郭冰),[2] Y. B. Wang (王友宝),[2] D. Y. Pang (庞丹阳),[3,4] J. Su (苏俊),[2] S. Q. Yan (颜胜权),[2] S. Zeng (曾晟),[2] L. Gan (甘林),[2] Z. C. Li (李志常),[2] J. C. Liu (刘建成),[2] X. X. Bai (白希祥),[2] Z. D. Wu (吴志丹),[2] S. J. Jin (金孙均),[2] L. Y. Zhang (张立勇),[5] X. Q. Yu (于祥庆),[5] L. Li (李龙),[5] H. B. Sun (孙慧斌),[1] G. Lian (连钢),[2] Q. W. Fan (樊启文),[2] and W. P. Liu (柳卫平)[2]

[1]*College of Physics Science and Technology, Shenzhen University, Shenzhen 518060, China*

[2]*China Institute of Atomic Energy, P.O. Box 275(10), Beijing 102413, China*

[3]*School of Physics and Nuclear Energy Engineering, Beihang University, Beijing 100191, China*

[4]*International Research Center for Nuclei and Particles in the Cosmos, Beihang University, Beijing 100191, China*

[5]*Institute of Modern Physics, Chinese Academy of Sciences, Lanzhou 730000, China*

(Received 8 August 2014; revised manuscript received 30 September 2014; published 22 December 2014)

The angular distributions of the ^{12}C(^{11}B, ^{11}B)^{12}C and ^{12}C(^{11}B, ^{12}C)^{11}B reactions have been measured at an incident energy of 50 MeV by using the high resolution Q3D magnetic spectrometer of the HI-13 tandem accelerator at China Institute of Atomic Energy, Beijing. The optical potential parameters of the ^{11}B + ^{12}C system are determined by fitting the angular distribution of the elastic scattering and then used to predict the cross sections of the elastic transfer reaction leading to the ground state in ^{12}C based on distorted-wave Born approximation (DWBA) analysis. Taking into account the interference between the elastic scattering and the elastic transfer processes, the proton spectroscopic factor of the ^{12}C ground state is extracted to be 2.15 ± 0.23 by constraining the geometrical parameters r_0 and a using the rms radius of the valence proton in the ^{12}C ground state.

DOI: 10.1103/PhysRevC.90.067601 PACS number(s): 25.70.Hi, 23.20.En, 21.10.Jx, 27.20.+n

The essential constituents of nuclear shell model are the single-particle orbits of the mean field which are occupied by protons and neutrons under the Pauli principle [1]. The spectroscopic factor is defined by a matrix element which describes the overlap between the initial and final states and yields the information on the occupancy of a given single-particle orbit [2]. It provides quantitative information about the single-particle structure of nuclei and plays an important role in a variety of topics on nuclear reaction and nuclear astrophysics.

The proton spectroscopic factor of the ^{12}C ground state is of special interest since it can be used in the calculation of the astrophysical ^{11}B(p, γ)^{12}C rate [3]. Shell model calculations done by Cohen-Kurath [4] in 1967 predicted the proton spectroscopic factor of the ^{12}C ground state to be $S_{^{12}\mathrm{C}} = 2.85$. After that, several experiments were performed through ^{12}C(e,$e'p$)^{11}B [5], ^{12}C(p,2p)^{11}B [6], ^{11}B(d,n)^{12}C [7], ^{12}C(d,^{3}He)^{11}B [8,9], ^{11}B(^{3}He,d)^{12}C [10,11], ^{11}B(^{7}Li,^{6}He)^{12}C [12], and ^{12}C(^{11}B, ^{12}C)^{11}B [13,14] reactions. The spectroscopic factors extracted from these measurements are different from each other in the range of 1.85 and 4.1.

Generally speaking, the elastic transfer reaction is regarded as a good tool for extracting spectroscopic factors since the spectroscopic factors as well as the distorted scattered waves are identical in both entrance and exit channels. Thus, the elastic transfer reaction enables the reduction of the uncertainty of the spectroscopic factor and has been frequently used to determine the neutron spectroscopic factor of ^{7}Li [15]; the proton spectroscopic factors of ^{9}Be [16], ^{10}B [17], ^{14}N [17], and ^{16}O [17]; the ^{3}He spectroscopic factor of ^{12}C [18]; and the ^{4}He spectroscopic factors of ^{7}Li [19] and ^{13}C[18].

For the ^{12}C(^{11}B, ^{12}C)^{11}B elastic transfer reaction, the angular distributions have been well reproduced by the distorted-wave Born approximation (DWBA) theory. However, there is still a remarkable discrepancy in the proton spectroscopic factor of the ^{12}C ground state [14]. It shows a smooth change with energy, and even exceeds the theoretical limit of $S_{\max} = 4.0$ between the energies of 8 and 36 MeV [13,14]. This abnormal behavior could not be explained by different reaction mechanisms and different distorted waves in model calculations [14]. However, all of the ^{12}C(^{11}B, ^{12}C)^{11}B angular distributions were measured using ΔE-E method with lower energy resolution so that the ^{13}C contaminant in the ^{12}C target was not taken into account. This might affect the measurement of ^{11}B + ^{12}C elastic scattering angular distributions, and thus disturb the optical potential parameters of the ^{11}B + ^{12}C system and the proton spectroscopic factors of ^{12}C ground state.

In the present work, the angular distributions of the ^{12}C(^{11}B, ^{11}B)^{12}C and ^{12}C(^{11}B, ^{12}C)^{11}B reactions were measured at an incident energy of 50 MeV by using the high resolution Q3D magnetic spectrometer. Compared to the ΔE-E method, the energy resolution of the Q3D magnetic spectrometer is as high as 0.02% [20], which is beneficial to the identification of reaction products and the elimination of the disturbance of the ^{13}C contaminant. The proton spectroscopic factor of the ^{12}C ground state was extracted by the comparison of experimental differential cross sections to the DWBA calculated ones.

*zhli@ciae.ac.cn

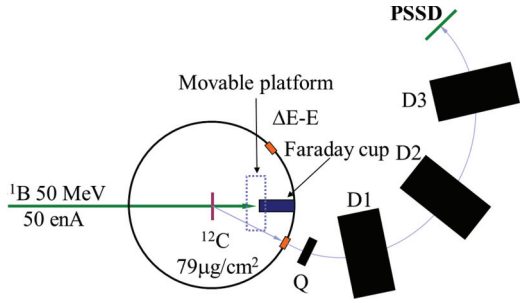

FIG. 1. (Color online) Schematic layout of the experimental setup.

The experiment was carried out at the HI-13 tandem accelerator of the China Institute of Atomic Energy (CIAE), Beijing. The experimental setup is shown in Fig. 1. A 50 enA ^{11}B beam with an energy of 50 MeV impinged on a self-supporting natural carbon target with a thickness of 79 μg/cm^2.

A Faraday cup was used to collect the beam for normalizing the cross sections at $\theta_{\rm lab} \geqslant 6^\circ$. The Faraday cup could be moved away when measuring the cross sections at $\theta_{\rm lab} \leqslant 6^\circ$. A ΔE-E telescope placed at $\theta_{\rm lab} = 25^\circ$ was employed for relative normalization of the cross sections at $\theta_{\rm lab} \leqslant 6^\circ$ by monitoring the recoiled ^{11}B particles from the ^{11}B + ^{12}C elastic scattering. In addition, the ratio of the current integration of the Faraday cup to the number of recoiled ^{11}B particles was measured at the start and end of the measurement for each angle of $\theta_{\rm lab} \leqslant 6^\circ$ by restoring the Faraday cup. The ratio changes by less than 2%, which indicates reliable normalization of the cross sections at $\theta_{\rm lab} \leqslant 6^\circ$.

A ϕ5 mm slit was placed at 240 mm far from the target, which results in a 0.34 mSr total solid angle and 0.25° angular error. Taking the ϕ3 mm beam spot into account, the angular errors attached to all of the cross sections are about 0.3°. In the measurements of the ^{12}C(^{11}B, ^{11}B)^{12}C and ^{12}C(^{11}B, ^{12}C)^{11}B reactions, the magnetic fields of Q3D magnetic spectrometer were set to focus ^{11}B and ^{12}C, respectively. After the reaction products were focused and separated by the Q3D magnetic spectrometer, they were measured by a 50 $\times$ 50 mm^2 two-dimensional position sensitive silicon detector (PSSD) which was placed on the magnetic spectrometer focal plane. The size of the PSSD enables the focused reaction products to be fully recorded.

The recoiled ^{11}B and ^{12}C particles were measured in the angular ranges of $8^\circ \leqslant \theta_{\rm lab} \leqslant 24^\circ$ and $3^\circ \leqslant \theta_{\rm lab} \leqslant 24^\circ$ in steps of about 1°, respectively. The typical two-dimensional spectrum of kinetic energy (E) versus the horizontal position (Px) and one-dimensional Px spectrum for the recoiled ^{11}B ions at $\theta_{\rm lab} = 15^\circ$ are shown in Fig. 2. One can see that the disturbance from the ^{13}C contaminant can be eliminated. The two-dimensional spectrum of E vs Px for the recoiled ^{12}C ions at $\theta_{\rm lab} = 15^\circ$ is shown in Fig. 3. At this angle, the energy of ^{12}C ions from the ^{13}C(^{11}B, ^{12}C)^{12}B reaction is 2.7% lower than that from the ^{12}C(^{11}B, ^{12}C)^{11}B reaction, the difference of the energy leads to a 134 mm distance which exceeds the size of PSSD. Thus, all of the ^{12}C ions in the box of Fig. 3 come from the ^{12}C(^{11}B, ^{12}C)^{11}B reaction.

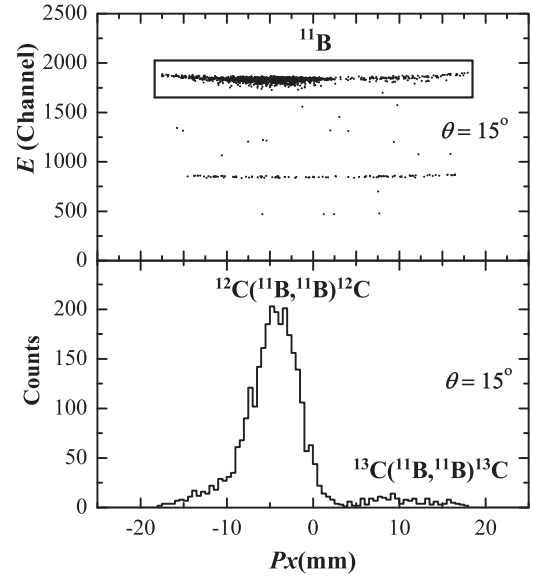

FIG. 2. Two-dimensional scatter plot of kinetic energy (E) vs horizontal position (Px) for the ^{12}C(^{11}B, ^{11}B)^{12}C elastic scattering, and the position spectrum of ^{11}B ions.

The angular distribution of the ^{11}B + ^{12}C elastic scattering at $E_{\rm c.m.} = 26.1$ MeV is obtained as shown in Fig. 4 together with the previous data [14] at the same energy. The data in forward and backward angles are obtained from the measurements of ^{11}B and ^{12}C ions, respectively. The errors of the differential cross sections are about 7%, mainly from the statistics and uncertainties of the target thickness. It can be seen clearly that the differential cross sections of the present work are 23% lower than the previous measurement [14] at backward angles of $\theta_{\rm c.m.} \geqslant 150^\circ$. This may indicate that the effect of the ^{13}C contaminant was successfully eliminated in the present work.

The events from elastic scattering and the elastic transfer reaction cannot be distinguished. Thus, the present angular distribution contains the contributions from the ^{12}C(^{11}B, ^{11}B)^{12}C and ^{12}C(^{11}B, ^{12}C)^{11}B reactions. In order to include the interference between elastic scattering and elastic transfer processes in the theoretical calculation, the elastic scattering amplitude $f^{\rm el}(\theta)$ was supplemented by the elastic transfer

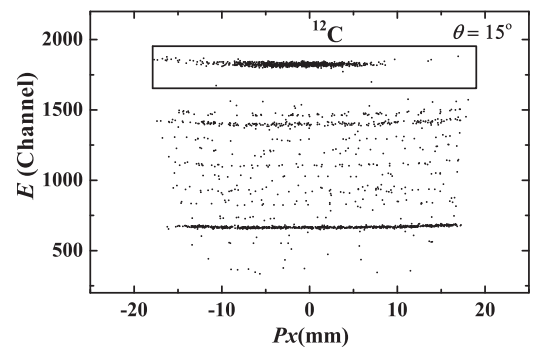

FIG. 3. Two-dimensional scatter plot of E vs Px for the ^{12}C(^{11}B, ^{12}C)^{11}B transfer reaction.

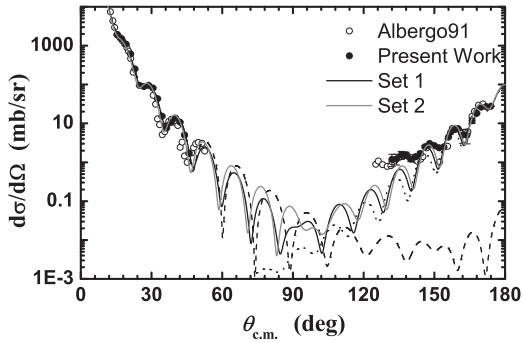

FIG. 4. Angular distribution of the ^{11}B+^{12}C elastic scattering reaction at $E_{\rm c.m.} = 26.1$ MeV which contains the elastic scattering and elastic transfer processes. The data with solid circles were measured in the present work and those with open circles were from Ref. [14]. The solid lines are the results of the DWBA calculation. The dotted and dashed lines denote the contributions of elastic transfer and elastic scattering processes, respectively.

amplitudes $f^{\rm tr}_{lm}(\pi-\theta)$ corresponding to the angular momentum transfer l and its projection m. The differential cross section was then expressed by[18]

$$\sigma(\theta) = \left|f^{\rm el}(\theta) + S_{^{12}\rm C} f^{\rm tr}_{00}(\pi-\theta)\right|^2 + S^2_{^{12}\rm C}\sum_{l\neq 0,m}\left|f^{\rm tr}_{lm}(\pi-\theta)\right|^2. \quad (1)$$

A DWBA code FRESCO [21] was utilized to analyze the angular distribution of the ^{12}C(^{11}B, ^{12}C)^{11}B reaction. The single-particle wave function of the bound state is obtained by solving the Schrödinger equation using a Woods-Saxon potential. The potential depth is determined to reproduce the valence proton binding energy of the ^{12}C ground state. The optical potential of the ^{11}B + ^{12}C system is extracted by fitting the present angular distribution with a Woods-Saxon form as

$$U(r) = -\frac{U_V}{1+\exp\left(\frac{r-R_R}{a_R}\right)} - i\frac{W_V}{1+\exp\left(\frac{r-R_I}{a_I}\right)} + U_C, \quad (2)$$

where

$$U_C = \frac{Z_P Z_T e^2}{2R_C}\left(3-\frac{r^2}{R_C^2}\right), \quad r \leqslant R_C, \quad (3)$$

$$= \frac{Z_P Z_T e^2}{r}, \quad r > R_C, \quad (4)$$

$$R_k = r_k\left(A_P^{1/3} + A_T^{1/3}\right), \quad k = R, I, C, \quad (5)$$

and Z_P, Z_T, and A_P, A_T are the numbers of charges and masses of the projectile and target, respectively.

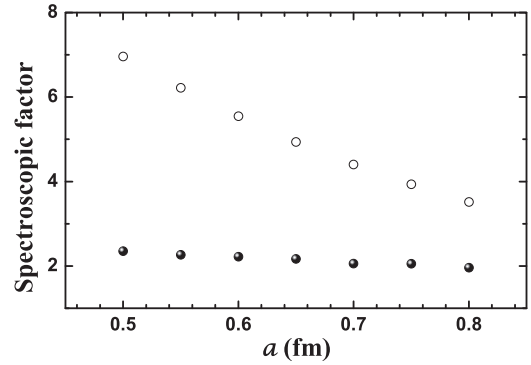

FIG. 5. Spectroscopic factor as a function of the diffuseness for the potential of ^{11}B + p bound state in ^{12}C. The solid circles denote the results obtained by constraining radius r_0 via by Eq. (8), while the open circles represent those without the r_v constraint.

The FRESCO program could automatically search the potential parameters and the proton spectroscopic factor of the ^{12}C ground state. For the experimental cross section $\sigma^{\rm expt}(\theta)$ with the absolute error $\Delta\sigma(\theta)$, the chi-square value χ^2 per point is obtained by [22]

$$\chi^2/N = \frac{1}{N}\sum_{i=1}^{N}\frac{[\sigma^{\rm th}(\theta) - \sigma^{\rm expt}(\theta)]^2}{\Delta\sigma(\theta)^2}, \quad (6)$$

where $\sigma^{\rm th}(\theta)$ is the DWBA theoretical cross section. The optimized potential parameters were obtained by fitting all of the ^{11}B + ^{12}C elastic scattering cross sections.

Two sets of optical potential parameters were employed in the DWBA calculations, as listed in Table I. The calculated angular distributions of the ^{11}B + ^{12}C elastic scattering are shown in Fig. 4. It can be seen that the experimental angular distribution was well reproduced. Figure 4 also exhibits the contributions of the elastic scattering and elastic transfer processes. The proton spectroscopic factor of ^{12}C ground state was determined to be 4.81 ± 0.24 and 5.06 ± 0.26 with the standard geometrical parameters $r_0 = 1.25$ fm and $a = 0.65$ fm. The uncertainties were mainly from the statistics of measurement.

In order to estimate the influence of the geometrical parameters on the proton spectroscopic factor of the ^{12}C ground state, the radius r_0 and diffuseness a were changed independently. When r_0 was changed from 1.1 to 1.4 fm and a was fixed at 0.65 fm, the spectroscopic factor varied from 7.00 to 3.46. And when a was changed from 0.5 to 0.8 fm and r_0 was fixed at 1.25 fm, the spectroscopic factor varied from 6.96 to 3.52 as shown in Fig. 5. The above changes led to more than 100% uncertainty of the deduced ^{12}C proton

TABLE I. Optical potential parameters used in the DWBA calculation. $E_{\rm in}$ denotes the incident energy in MeV. The potentials have a Wood-Saxon form, where U_V, r_R, and a_R are the depth, radius, and diffuseness of the real potentials; and W_V, r_I, and a_I are those for the imaginary potentials. U and W are in MeV, r and a are in fm. χ^2/p denotes the reduced chi-square value (χ^2 per point).

Set no.	$E_{\rm in}$	U_V	r_R	a_R	W_V	r_I	a_I	r_C	χ^2/p	$S_{^{12}\rm C}$	Ref.
Set1	50.0	70.05	1.06	0.55	26.27	1.06	0.71	1.00	4.54	4.81 ± 0.24	Present work
Set2	50.0	60.50	1.09	0.61	36.04	1.18	0.49	1.00	22.22	5.06 ± 0.26	[14]

TABLE II. Theoretical and experimental proton spectroscopic factors of the ^{12}C ground state.

$S_{^{12}C}$	Expt. or Theor.	Ref.
2.85	Theory	[4]
1.85 ± 0.03	^{12}C(e, $e'p$)^{11}B	[5]
2.0 ± 0.2	^{12}C(p,2p)^{11}B	[6]
1.85 ± 0.05	^{11}B(d,n)^{12}C	[12]
2.125	^{12}C(d,^{3}He)^{11}B	[11]
4.10	^{11}B(^{7}Li,^{6}He)^{12}C	[12]
2.15 ± 0.23	^{12}C(^{11}B, ^{12}C)^{11}B	Present work

spectroscopic factor, therefore reliable geometrical parameters are needed.

The root-mean-square (rms) radius r_v of the valence proton orbit in ^{12}C can be calculated by

$$r^2_{^{12}C} = \frac{1}{Z+1}\left(Zr^2_{^{11}B} + r^2_p + \frac{Z}{Z+1}r^2_v\right), \quad (7)$$

where $r_{^{12}C}$ = 2.46 fm [23], $r_{^{11}B}$ =2.38 fm [24], and r_p = 0.8768 fm [25] are the charge rms radii for ^{12}C, ^{11}B, and proton, respectively. Z denotes the proton number in ^{11}B. According to the shell model, r_v can be reproduced by

$$r_v = \left(\frac{\int_0^\infty r^4[\phi(r)]^2dr}{\int_0^\infty r^2[\phi(r)]^2dr}\right)^{1/2}, \quad (8)$$

where $\phi(r)$ is the single-particle wave function of the ^{11}B + p bound state in ^{12}C which can be calculated by solving the Schrödinger equation with Woods-Saxon potential. The a was changed from 0.5 to 0.8 fm while r_0 was adjusted to reproduce the rms radius of the valence proton in ^{12}C by Eq. (8). The extracted spectroscopic factor as a function of a is shown in Fig. 5. One can see that the uncertainty was reduced to be 10%, and the proton spectroscopic factor of the ^{12}C ground state was determined to be 2.15 ± 0.23 with r_v constraint. The uncertainties are mainly from the statistics of measurement (5%), the divergence of optical potential parameters (3%), and the variation of geometrical parameters (9%).

The spectroscopic factors obtained in theoretical and several experimental investigations are listed in Table II. After constraining r_0 and a, our result is in agreement with those derived from the ^{12}C(p,2p)^{11}B [6], ^{11}B(d,n)^{12}C [7], and ^{12}C(d, ^{3}He)^{11}B [11] reactions.

In summary, the angular distributions of the ^{11}B+^{12}C elastic scattering and elastic transfer reaction have been measured at $E(^{11}B)$ = 50 MeV with the high resolution Q3D magnetic spectrometer of HI-13 tandem accelerator at CIAE, Beijing. Since the geometrical parameters r_0 and a have a big influence on the proton spectroscopic factor of the ^{12}C ground state, we constrain the r_0 and a by reproducing the rms radius of the valence proton in the ^{12}C ground state. The proton spectroscopic factor of the ^{12}C ground state is extracted to be 2.15 ± 0.23 which is in agreement with those derived from the ^{12}C(p,2p)^{11}B, ^{11}B(d,n)^{12}C, and ^{12}C(d,^{3}He)^{11}B reactions. The present approach can be extensively utilized to study the spectroscopic factors, and is particularly effective for the case of the bound state with nonstandard geometrical parameters.

We thank the staff of HI-13 tandem accelerator for the smooth operation of the machine. This work is supported by the National Natural Science Foundation of China under Grants No. 11321064, No. 11375269, and No. 11205247, the 973 program of China under Grant No. 2013CB834406, and the Natural Science Foundation of SZU under Grant No. 00035691.

[1] E. Caurier, G. Martínez-Pinedo, F. Nowacki, A. Poves, and A. P. Zuker, Rev. Mod. Phys. **77**, 427 (2005).
[2] M. H. Macfarlane and J. B. French, Rev. Mod. Phys. **32**, 567 (1960).
[3] C. Angulo, M. Arnould, M. Rayet *et al.*, Nucl. Phys. A **656**, 3 (1999).
[4] S. Cohen and D. Kurath, Nucl. Phys. A **101**, 1 (1967).
[5] L. Lapikás, G. van der Steenhoven, L. Frankfurt, M. Strikman, and M. Zhalov, Phys. Rev. C **61**, 064325 (2000).
[6] D. W. Devins, D. L. Friesel, W. P. Jones *et al.*, Aust. J. Phys. **32**, 323 (1979).
[7] G. S. Mutchler, D. Rendić, D. E. Velkley, W. E. Sweeney, and G. C. Phillips, Nucl. Phys. A **172**, 469 (1971).
[8] M. Gaillard, R. Bouché, L. Feuvrais *et al.*, Nucl. Phys. A **119**, 161 (1968).
[9] F. Hinterberger, G. Mairle, U. Schmidt-Rohr, P. Turek, and G. J. Wagner, Nucl. Phys. A **106**, 161 (1968).
[10] P. D. Miller, J. L. Duggan, M. M. Duncan *et al.*, Nucl. Phys. A **136**, 229 (1969).
[11] G. M. Reynolds, D. E. Rundquist, and R. M. Poichar, Phys. Rev. C **3**, 442 (1971).
[12] G. H. Neuschaefer, M. N. Stephens, S. L. Tabor, and K. W. Kemper, Phys. Rev. C **28**, 1594 (1983).
[13] L. Jarczyk, B. Kamys, A. Strzalkowski *et al.*, Phys. Rev. C **31**, 12 (1985).
[14] S. Albergo, S. Costa, R. Potenza *et al.*, Phys. Rev. C **43**, 2704 (1991).
[15] J. Su, Z. H. Li, B. Guo *et al.*, Chin. Phys. Lett. **27**, 052101 (2010).
[16] O. Camargo, V. Guimarães, R. Lichtenthäler *et al.*, Phys. Rev. C **78**, 034605 (2008).
[17] J. Sromicki, M. Hugi, J. Lang *et al.*, Nucl. Phys. A **406**, 390 (1983).
[18] L. Jarczyk, J. Okolowicz, A. Strzalkowski *et al.*, Nucl. Phys. A **316**, 139 (1979).
[19] V. Guimaraes, R. Z. Denke, R. Lichtenthäler *et al.*, AIP Conf. Proc. **1098**, 219 (2009).
[20] Z. C. Li, Y. H. Cheng, C. Yan *et al.*, Nucl. Instrum. Methods Phys. Res. A **336**, 150 (1993).
[21] I. J. Thompson, Comput. Phys. Rep. **7**, 167 (1988).
[22] I. J. Thompson and F. M. Nunes, *Nuclear Reactions for Astrophysics* (Cambridge University, New York, 2009).
[23] I. Sick and J. S. McCarthy, Nucl. Phys. A **150**, 631 (1970).
[24] A. Olin, P. R. Poffenberger, G. A. Beer *et al.*, Nucl. Phys. A **360**, 426 (1981).
[25] P. J. Mohr, B. N. Taylor, and D. B. Newell, Rev. Mod. Phys. **80**, 633 (2008).